Dendrimer Templates for the Formation of Gold Nanoclusters

Franziska Gröhn, Barry J. Bauer, Yvonne A. Akpalu, Catheryn L. Jackson, and Eric J. Amis*

Polymers Division, National Institute of Standards and Technology, Gaithersburg, Maryland 20899

Received January 28, 2000; Revised Manuscript Received June 8, 2000

ABSTRACT: Charged poly(amidoamine) (PAMAM) dendrimers are used to create organic−inorganic hybrid colloids in aqueous solution. The formation of gold colloids upon reduction of a gold salt precursor serves as a model reaction to study the influence of reaction conditions and dendrimer generation on the resulting nanostructures. Characterization by transmission electron microscopy (TEM), small-angle neutron scattering (SANS), and small-angle X-ray scattering (SAXS) show that the gold particles are formed inside the dendrimer and located offset from the center. Although lower generation dendrimers aggregate when stabilizing the metal particles formed, dendrimers of generation 6−9 can template one gold colloid per dendrimer molecule, the size of which is well-controlled by the number of gold atoms added per dendrimer. For generation 10, multiple smaller gold particles per dendrimer are observed. The effectiveness of PAMAM dendrimers as templates in the host−guest nanoscale synthesis is confirmed for different chemical reactions.

I. Introduction

Organic−inorganic hybrid nanostructures have generated great interest due to the combination of the colloidal properties of inorganic crystals with mechanical properties or functionalities of organic compounds, resulting in a variety of potential applications as electrical, optical, medical, and information storage materials. To design such hybrid nanostructures, templating a growing inorganic crystal within a polymeric matrix, a method that was initially inspired by nature, has been evaluated as an effective synthetic route for a variety of systems.[1]

Dendrimers, well-defined polymer molecules that are known to act as hosts for guest molecules,[2,3] are a new type of potential template for the formation of inorganic nanoclusters. Recently, Crooks,[4] Esumi,[5] and Balogh[6] have discovered the ability of dendrimers to form organic−inorganic nanocomposites, and already a number of further reports have followed.[7−15] The first studies show that the reduction of copper[4,6] or gold[5] ions in the presence of generation 4 (G4) PAMAM dendrimer leads to stable colloidal solutions, rather than macroscopic metal precipitates. UV−vis spectroscopy confirms the formation of nanometer-scale copper particles.[4,6] In addition, it has recently been shown by TEM that relatively monodisperse platinum and palladium colloids can be formed.[8] Several exciting applications of these dendrimer−inorganic hybrid materials have already been considered. The dendrimer-stabilized nanoclusters have been demonstrated to be effective high surface area catalysts in solution that allow substrates to penetrate the dendrimer interior and access the cluster surface.[11] In contrast to classical metal colloids in solution, the unique architecture of the stabilizing dendrimer allows for a remarkable selectivity of such catalysts, as was shown by Crooks et al. for the hydrogenation of alkenes in water.[8,16] Furthermore, the dendrimers can be immobilized to electrode surfaces and serve as electrocatalysts for O_2 reduction.[11]

However, our motivation for using dendrimers comes from a somewhat different perspective: the desire to understand the general features of polymer nanotemplating with a model system. The success of organic−inorganic hybrid materials requires the study of fundamentals such as a characterization of the nanostructure, formation mechanisms, and properties. Here, dendrimers can offer a unique advantage over conventional polymer systems. Dendrimers are monodisperse and well-characterized molecules with a size in a range of 1−15 nm for generation 2−10 (G2−G10),[17] spanning characteristic sizes of low molecular mass molecules, polymers, and colloids. Dendrimers are a *mesoscopic* model system.

In this study, we investigate poly(amidoamine) (PAMAM) dendrimers of G2−G10 as potential nanotemplates for the formation of inorganic−organic hybrid colloids in aqueous solution (whereas previous reports employed low generation dendrimers, G6 and below). Our approach relies on the attraction between charged dendrimers and oppositely charged metal ions. Performing chemical reactions on these precursor ions that are associated with the dendrimer should produce colloid structures that are controlled by the dendrimer. The concept of using charged, solvent-penetrable nanopolymer−particles as templates in aqueous solution was first applied to polyelectrolyte microgels.[18] It has also been applied for G2 and G4 dendrimers,[5] but most of the previous studies used a specific coordination chemistry for the attachment of precursor ions to the dendrimer amine groups.[4,6] In this study, we use the reduction of gold with sodium borohydride as a classical model reaction, since for this reaction it is known how to influence the reaction speed, one of the critical factors of colloid formation.[18] Transmission electron microscopy (TEM), small-angle neutron scattering (SANS), and small-angle X-ray scattering (SAXS) are employed to characterize the nanoscale structures of the resulting organic−inorganic hybrids.

II. Experimental Section

A. Synthesis. Poly(amidoamine) (PAMAM) dendrimers of generations 2−4 were purchased from Aldrich Chemical Co., and generations 5−10 were supplied by Dendritech (Michigan Molecular Institute).[19] Aqueous solutions with a dendrimer mass fraction of 0.1−1% were prepared by diluting concen-

10.1021/ma000149v
Published on Web 07/18/2000

trated dendrimer/methanol solutions (dendrimer mass fraction of 20−25%) with deionized water. Dilute aqueous solutions of PAMAM dendrimers were mixed with aqueous solutions of $HAuCl_4$ at controlled stoichiometries. After stirring these solutions for 1 h, sodium borohydride in basic aqueous solution (0.025−0.5 M sodium hydroxide[20]) was added. The light yellow dendrimer/ $HAuCl_4$ solutions immediately turned brown or red, indicating the formation of colloidal gold.

UV−vis spectra of the dendrimer−gold colloid solutions were obtained on a Perkin-Elmer Lambda 9-spectrometer in the wavelength range of 400−800 nm. TEM was also performed on these solutions as well as on dialyzed samples. The resulting TEM images for both cases are the same. For the SANS experiments, samples were either dialyzed against deuterium oxide or directly synthesized in deuterium oxide.

B. Characterization. 1. Transmission Electron Microscopy (TEM). Carbon-coated copper grids, 300 mesh, were washed in chloroform reflux in order to remove Formvar. Grids were then treated for 2−5 s in a glow-discharge tube in partial vacuum to impart hydrophilic character to the carbon substrate. Stained specimens were prepared by depositing the sample solutions on the grid and inverting the grid on a drop of aqueous phosphotungstic acid solution that had been neutralized with NaOH (2% mass fraction of phosphotungstic acid). The grid was then blotted on filter paper and air-dried. TEM images were obtained at 120 kV with a Philips 400 T at a magnification of 46 000× and 100 000×. The relative error is within 10% of the magnification.

2. Small-Angle Neutron Scattering (SANS). Samples for SANS measurements were transferred into optical quality quartz banjo cells with 2 mm path length. SANS studies were performed at the Center for Neutron Research at the National Institute of Standards and Technology.[21] Measurements were made using the 30 m SANS instrument with a neutron wavelength $\lambda = 0.6$ nm and wavelength spread of $\Delta\lambda/\lambda = 0.15$. Data were corrected for empty quartz cell scattering, electronic background, and detector uniformity and converted to an absolute scale using secondary standards. The data were further corrected by subtracting the contributions from solvent scattering and incoherent background.

3. Small-Angle X-ray Scattering (SAXS). SAXS data were collected at the Advanced Polymer Beamline at Brookhaven National Laboratory, X27C. The radiation spectrum from the source was monochromated using a double multilayer monochromator and collimated with three 2° tapered tantalum pinholes to give an intense X-ray beam at $\lambda = 1.307$ Å.[22] Two configurations were used with a linear position sensitive detector (European Molecular Biology Laboratory, EMBL) or a 2D image plate detector (BAS2000, Fuji). The sample-to-detector distance was varied between 1 and 1.5 m. A vacuum chamber was placed between the sample and detector to reduce air scattering and absorption. The span of scattering vector magnitudes ($q = (4\pi/\lambda)\sin(\theta)$ and 2θ the scattering angle) was in the range 0.15 $nm^{-1} < q < 3.2$ nm^{-1} and 0.2 $nm^{-1} < q < 4.4$ nm^{-1} for the two configurations used. Scattering patterns from silver behenate and Lupolen were used for angular calibration of the detectors. A parallel plate ionizing detector placed before the sample cell was used to record the incident intensities. The experimental intensities were corrected for incident intensity and for background scattering from the camera and empty cell. The correction for pixel-by-pixel detector sensitivity was established from the scattering by an Fe-59 source.

The two-dimensional data were circularly averaged. Uncertainties were calculated from the standard deviation of the pixel statistics in the averaged annulus. The scattering curves presented here were obtained by further averaging three to four individual measurements. The uncertainties are the standard deviations of the mean intensity and are plotted only when the uncertainty limits are larger than the size of the plotted data points. All scattering intensities were corrected for solvent scattering.

The scattering curve $I(q)$ was Fourier transformed into the pair distance distribution function $P(r)$ using the program ITP (*Indirect Transformation for the Calculation of* $P(r)$) by Glatter.[23−25] This includes smoothing of the primary data by a weighted least-squares procedure (estimation of the optimum stabilization parameter based on a stability plot) and transformation into real space by the indirect transformation method with minimized termination effects.

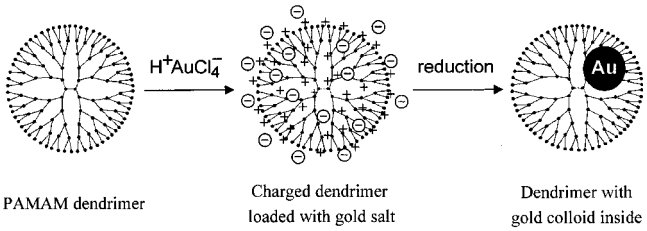

Figure 1. Dendrimer nanotemplating in aqueous solution. In a first step, the dendrimer is loaded with a precursor salt ($H^+AuCl_4^-$), resulting in a charged dendrimer with the precursor as counterions. In a second step, the chemical reduction is performed which yields a colloid inside the dendrimer.

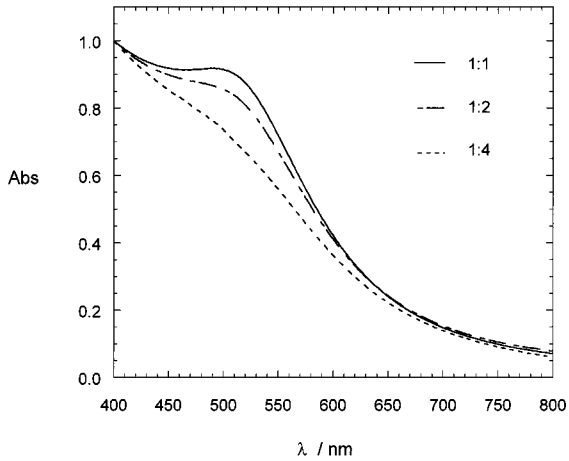

Figure 2. UV−vis spectra for gold−dendrimer hybrid colloids in aqueous solution. The spectra correspond to G9−PAMAM dendrimer samples loaded with different amounts of gold. (The molar ratio of gold ions to dendrimer end groups is indicated in the legend.)

III. Results and Discussion

A. Nanocomposite Synthesis. The nanotemplating by dendrimers in aqueous solution is depicted schematically in Figure 1. The addition of $HAuCl_4$ to a neutral dendrimer with primary and tertiary amine groups results in a protonated dendrimer with $AuCl_4^-$ counterions. The gold ions are then reduced to metallic gold without the formation of a macroscopic metal precipitate. The stable brown to red solutions of colloidal gold formed indicate that the metal colloids were stabilized by the dendrimer. The brown or red color of the solutions and UV−vis spectra (Figure 2) are typical of gold colloids in the size range of 1−5 nm. In the following discussion, we will show that the location of the gold colloid inside the dendrimer as sketched in Figure 1 is an accurate representation of the dendrimer−colloid structure.

B. Optimization of the Reaction Conditions. The stabilization of gold colloids in aqueous solution by the PAMAM dendrimers is possible over a wide range of reaction conditions. To control the size of the particles, one needs to optimize the ratio of the added gold ions to dendrimer, the dendrimer concentration in solution, and the reduction rate.

In the first step, the gold/dendrimer ratio has to be adjusted so that no precipitation occurs. We found that gold could be added to the solution without precipitation

of the dendrimer up to the amount corresponding to a gold salt to dendrimer end group ratio of 1:1. It is important to emphasize that we refer to the number of end groups as a reference value only and do not imply any specific binding to the end groups. The dendrimer contains an equivalent number of inner, tertiary amine groups, which can also be protonated and thereby attract $AuCl_4^-$ counterions. We also note that a number of previous studies investigated the coordination of metal ions such as Cu^{2+} and Pd^{2+} to inner and outer dendrimer amine groups by EPR and UV−vis spectroscopy,[4,6,26−28] showing that the metal ions can be coordinated to outer primary as well as inner tertiary dendrimer amine groups, i.e., can be located inside the dendrimer. In general, $AuCl_4^-$ ions do not show any specific coordination to amine groups, but it has been shown previously that electrostatic attraction of precursor ions to polyelectrolyte microgels is sufficient to allow for effective nanotemplating.[18] We note that this study is focused on characterization of the resulting hybrid particles after reduction, rather than the precursor complex.

At higher concentration (dendrimer mass fraction ≥2%), precipitation occurs upon reduction of the gold salt. Encapsulation of the metal colloid in individual dendrimers cannot be proven by the absence of precipitation, but the absence of precipitation is a necessary condition. When the concentration of the dendrimer is sufficiently low (for example, a dendrimer mass fraction of 1%), a stable colloidal solution is formed, but the resulting gold colloids are relatively polydisperse, as is observed by TEM. It is only when the dendrimer mass fraction is 0.12% or lower that the reduction can result in uniform gold colloids. Therefore, we employ a dendrimer mass fraction of 0.12% for all subsequent experiments.

The third parameter to be optimized is the reaction rate, i.e., mass transfer and growth in comparison to nucleation. We performed the reduction with sodium borohydride in order to control the reduction rate by the pH of the solution.[18] If the reduction is fast ($NaBH_4$ in 0.025−0.1 M NaOH), again polydisperse colloids and partly multiple colloids within one dendrimer are observed (Figure 3a). For slower reduction rates ($NaBH_4$ in 0.3 M NaOH), uniform encapsulated particles can be formed (Figure 3b). Under much slower reduction conditions ($NaBH_4$ in 0.4 M NaOH), a red-violet precipitate is observed. Thus, the dendrimer is an effective template only when sufficiently slow reduction rates are used. This trend corresponds to results for other systems, but the specific optimal conditions are different.[18,29] We have chosen the slowest reduction that results in stable colloidal solutions ($NaBH_4$ in 0.3 M NaOH) for further investigations, hereafter referred to as "slow reduction". Furthermore, the precipitate obtained at even slower reduction is also a dendrimer−metal composite material since the color indicates nanometer dimensions of the metal. Precipitation may occur from the reduction of dendrimer charge via the pH of the reducing solution. However, while this complex material is an interesting hybrid system, it is not the focus of this study.

C. Characterization of the Hybrid Particles. The particles synthesized are investigated by TEM, SANS, and SAXS. The characterization procedure is demonstrated for a representative G9−gold sample (loading ratio 1:1, slow reduction) in this section.

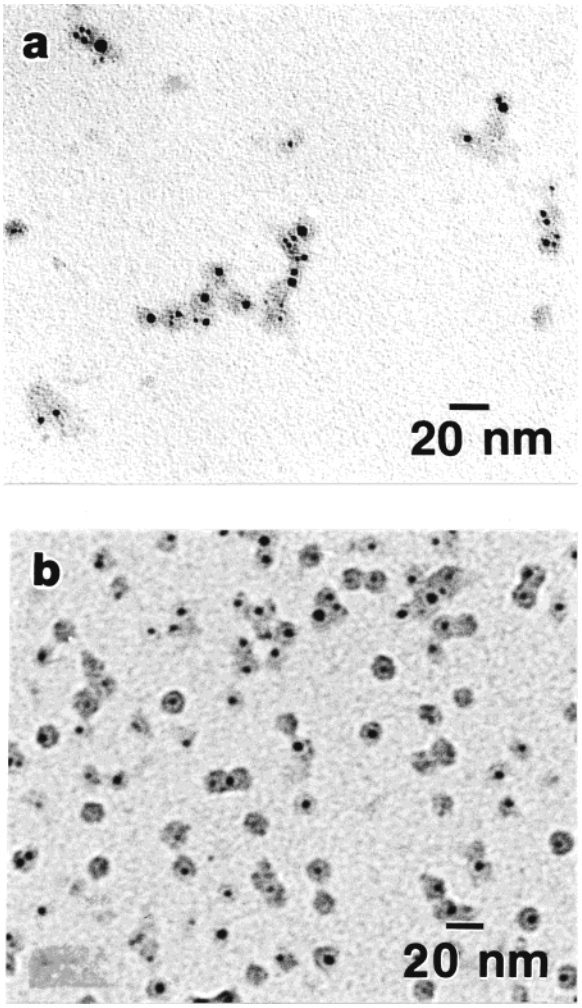

Figure 3. TEM of gold containing G9 PAMAM dendrimer obtained for 1:1 loading. The dendrimers have been stained with phosphotungstic acid and appear gray; the gold colloids appear black. (a) Fast reduction ($NaBH_4$ in 0.1 M NaOH); (b) slow reduction ($NaBH_4$ in 0.3 M NaOH).

TEM on the dendrimer−gold particles was performed after staining the dendrimer; thus, both components are evident in Figure 3b. The image indicates that the colloid particles are formed inside the dendrimer. Under these slow reaction conditions, one gold particle per dendrimer is predominantly formed. The gold colloids observed are relatively monodisperse. The sizes estimated for the dendrimer and gold are 13 and 4 nm, respectively. The measured dendrimer size corresponds to previous reports of the size of the unmodified PAMAM dendrimers.[17,30]

The TEM image in Figure 3b suggests that some of the dendrimers aggregate. From the TEM experiments one cannot determine whether the aggregates are present in the parent solution or formed while casting on the grid. Solution characterization methods must be applied to resolve this issue.

SANS measurements were performed on solutions of the dendrimer−gold hybrid particles in deuterium oxide. Scattering curves for the unmodified dendrimer and the gold containing dendrimers are shown in Figure 4. For the dendrimer−gold hybrid particles, the radius of gyration obtained from Guinier extrapolation is 5.1 ± 0.1 nm. This is within the experimental error the same as for the unmodified dendrimer. The result indicates that the hybrid particles also do not form larger ag-

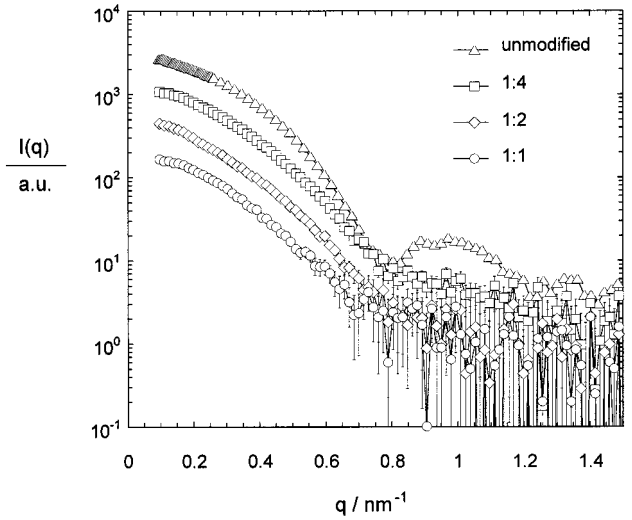

Figure 4. Small-angle neutron scattering curves $I(q)$ for the unmodified G9 PAMAM dendrimer and gold containing G9 PAMAM dendrimers obtained for different loading ratios 1:1, 1:2, and 1:4. Error bars are the standard deviations of the mean intensity. Scattering curves were shifted in order to allow for a better comparison and thus do not represent absolute intensities in this plot.

gregates in solution. Furthermore, the higher order sphere form factor features, which are pronounced in the case of the unmodified dendrimer, nearly completely disappear for the hybrid samples. This will be understood in the context of the SAXS results.

SAXS provides more detailed information about the colloid structures. In Figure 5, data for an unmodified G9 dendrimer are shown. Figure 6 shows data for dendrimer−gold hybrid particles, which correspond to the TEM sample in Figure 3b. The scattering curves $I(q)$ (Figures 5a and 6a) can be Fourier transformed, yielding the pair distance distribution functions $P(r)$ (Figures 5b and 6b). Transformation into real space, which does not include geometric assumptions about the particle, demonstrates the different particle features more obviously than the inverse space scattering curves, in this case. The shape of the $P(r)$ for the unmodified dendrimer in Figure 5b corresponds to a homogeneous sphere of 13 nm diameter, which is in agreement with earlier modeling results.[17] In contrast, the shape of the $P(r)$ for the hybrid particle in Figure 6b is typical of a layered sphere. An estimate of the dimensions of the inner-sphere and outer-sphere diameter confirms the diameters of the gold (4 nm) and the dendrimer (13 nm) estimated from TEM. More importantly, this result proves that the gold is formed inside the dendrimer.

A further deconvolution of the pair distance distribution function $P(r)$ under the assumption of a specific geometry (which has been deduced from the $P(r)$ function itself) generally leads to the particle electron density profile, $\rho(r)$. In the case of the hybrid particles (Figure 6), by assuming spherical symmetry, a satisfactory description of the $P(r)$ function, specifically the relative peak heights, is not possible. Deviation from strict spherical particle symmetry is one possible reason for such a discrepancy.

Additional modeling has been performed in order to understand this issue: We calculated the scattering curves and the pair distance distribution functions for several model layered particles. At this point, one can compare the scattering curves or the real-space pair distance distribution functions in order to understand

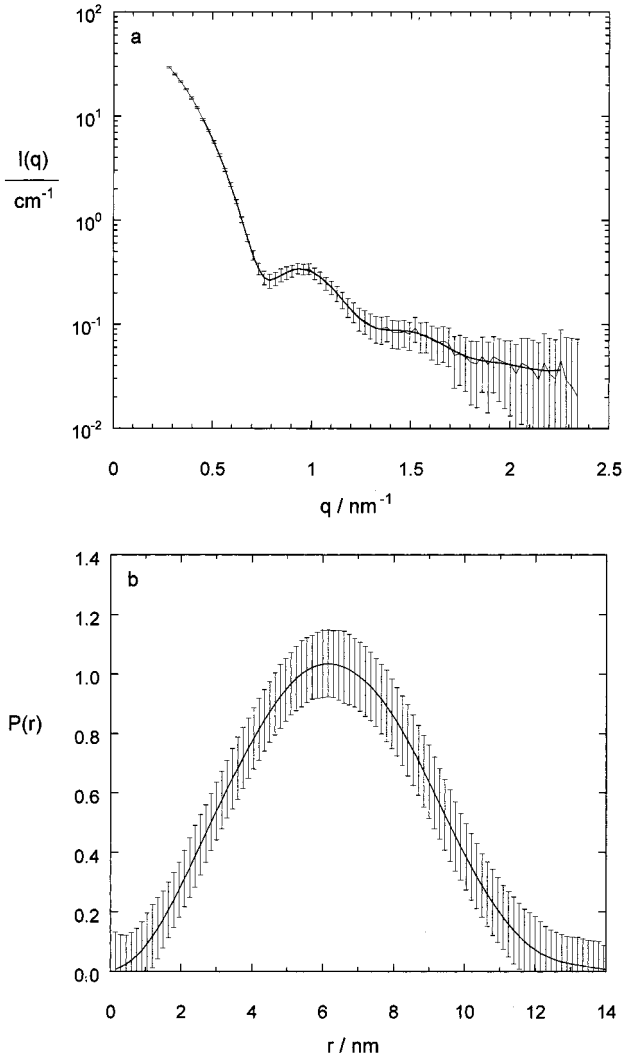

Figure 5. (a) Small-angle X-ray scattering curve $I(q)$ for the unmodified G9 PAMAM dendrimer along with fit to the data. Error bars are the measured standard deviation in $I(q)$. (b) Pair distance distribution function $P(r)$ obtained by indirect Fourier transformation of the scattering data $I(q)$ (program ITP). A homogeneous sphere structure with a diameter of 13 nm becomes evident. Error bars are the standard deviation in the estimation of $P(r)$, which results from the fit to the $I(q)$ data in (a).

the basic trends. We will refer to the pair distance distribution functions here, since the effects are more obvious. Figure 7a displays the calculated pair distance distribution functions for layered spheres with different relative contrast of the inner sphere. The variation does not allow the modeling of the basic shape of the experimental pair distance distribution function (Figure 6b). This points to deviations from a perfect spherical symmetry, as was already indicated by the problem with the deconvolution of the $P(r)$. When considering potential structures with nonspherical symmetry, one has to remember that the maximal diameters of the unmodified dendrimer and the gold-containing dendrimer are the same (Figures 5b and 6b). Thus, the best hypothesis for nonspherical symmetry in our system is a noncentered placement of the gold particle within the dendrimer. In Figure 7b we calculated pair distance distribution functions for layered particles with constant relative contrast, but an increasing offset of the inner sphere from the center of the outer sphere. Agreement between calculated and experimental $P(r)$ cannot be

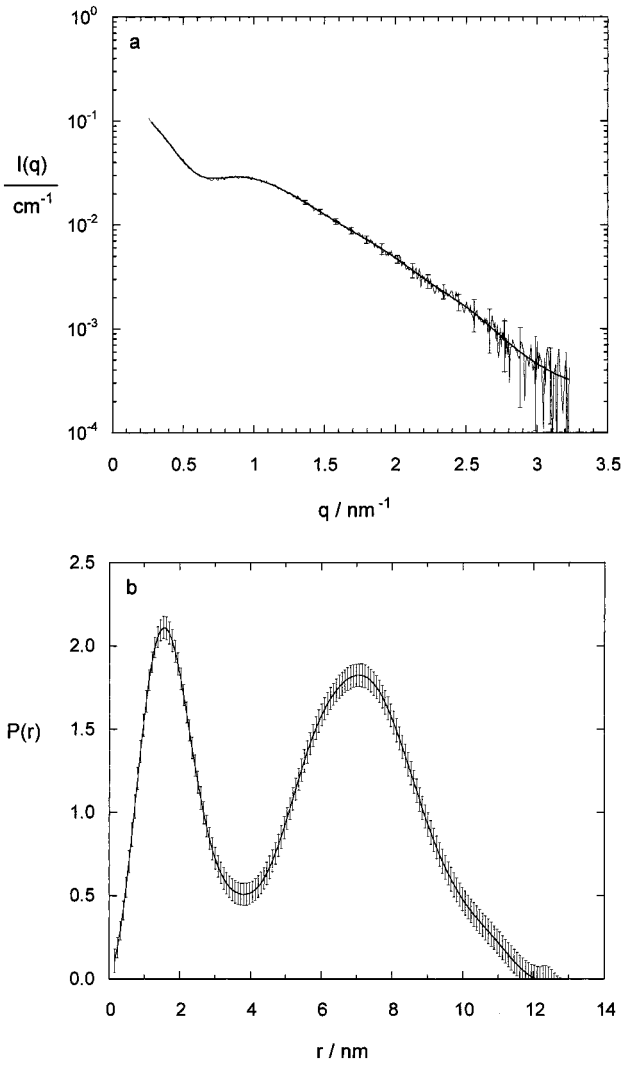

Figure 6. (a) Small-angle X-ray scattering curve $I(q)$ for the gold containing G9 PAMAM dendrimer of Figure 3b along with fit to the data. The relative standard deviation in the SAXS intensity values in the range 0.3 $nm^{-1} < q < 1.4$ nm^{-1} is less than 3% and lies within the thickness of the line. At higher wavevectors, the relative standard deviation increases with q, and error bars are plotted, which are the measured standard deviation in $I(q)$, for every 10th data point. (b) Pair distance distribution function $P(r)$ obtained by indirect Fourier transformation of the scattering data $I(q)$ (program ITP). A layered-sphere structure with a total diameter of 13 nm becomes evident. Error bars are the standard deviation in the estimation of $P(r)$, which results from the fit to the $I(q)$ data in (a).

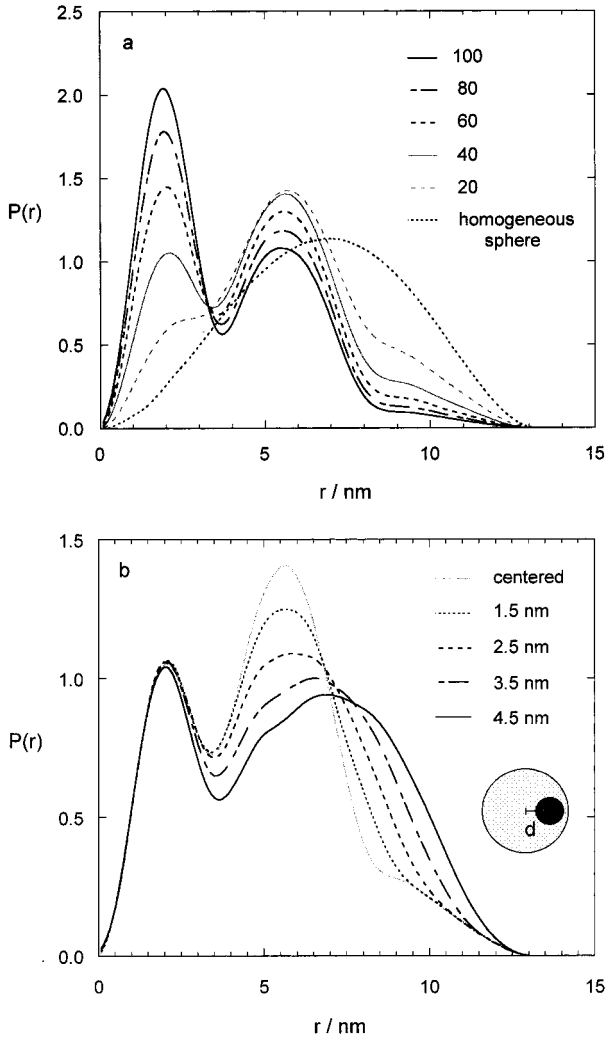

Figure 7. (a) Theoretical pair distance distribution function $P(r)$ calculated for layered spheres with different relative contrast of the inner sphere (solvent contrast = 0, outer sphere contrast = 1, inner sphere contrast as given in the figure). The basic shape of the experimental function in Figure 6b cannot be modeled. (b) Theoretical pair distance distribution function $P(r)$ calculated for layered spheres with different offset of the inner sphere inside the outer sphere (outer-sphere radius = 6.6 nm, inner-sphere radius = 1.8 nm, relative contrast 40, offset d between centers given in the figure). The basic shape of the experimental function is best represented for an offset of 3.5−4.5 nm.

quantitative because of effects of polydispersity in colloid size and offset. However, the experimental pair distance distribution function (Figure 6b) can only be represented with an offset of 3.5−4.5 nm (Figure 7b). Therefore, it is clear that the gold particle is offset from the center of the dendrimer.

The displacement of the gold from the dendrimer center is also visible in some of the particles in the TEM in Figure 3b. (Because the TEM is a two-dimensional projection, only a fraction of the gold colloids appears off-centered.) In addition, this off-center placement of the gold in relation to the dendrimer can also explain the loss of sharp features in the SANS scattering curve shown above.

Thus, we have shown that the gold colloid is inside the dendrimer, and it is located with an offset from the center as was depicted schematically in Figure 1. The good agreement between the gold colloid diameter determined from TEM and SAXS allows a quantitative comparison with the model sketched: The G9 dendrimer was loaded with gold salt corresponding to a gold ion to end group ratio of 1:1, i.e., 2048 gold ions per dendrimer molecule. Assuming the formation of one gold colloid from the loading of one dendrimer molecule upon reduction, one would expect a gold particle consisting of 2048 gold atoms. This means an expected particle size of 4 nm when assuming bulk density for the gold. This calculated value is in good agreement with the experimental results. Thus, the postulate that the gold ions from the load of one dendrimer form one particle has been demonstrated to be true. The gold colloid formation is indeed templated by the dendrimer. We will hereafter refer to this template mechanism as “fixed loading law”.

D. Influence of the Gold to Dendrimer Loading Ratio. As stated above, the maximal loading of the dendrimer with gold (1:1 molar ratio of gold ions to

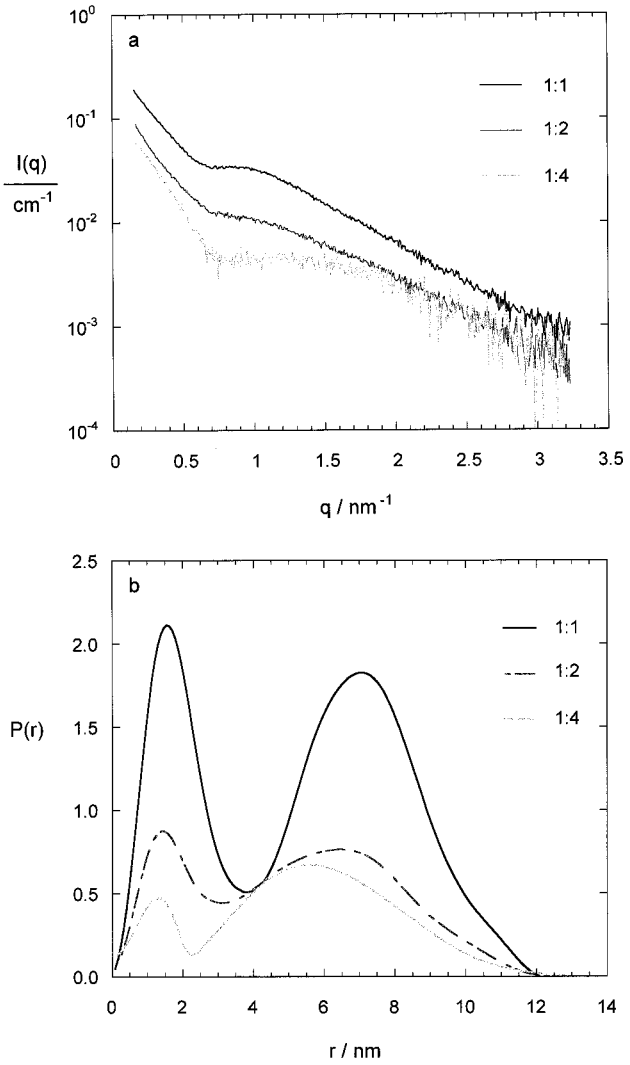

Figure 8. (a) Small-angle X-ray scattering curves $I(q)$ for gold containing G9 PAMAM dendrimers obtained for different loading ratios 1:1, 1:2, and 1:4. The relative standard deviation in the SAXS intensity values in the range 0.2 $nm^{-1} < q < 2.0$ nm^{-1} is less than 3%. At higher wavevectors, the relative standard deviation increases with q to a maximum value of 10%. (b) Pair distance distribution functions $P(r)$ obtained by indirect Fourier transformation of the scattering data $I(q)$ in (b). The decreasing gold diameter but constant dendrimer diameter upon decreasing loading is visible. The relative standard deviation in the $P(r)$ values is less than 3%.

dendrimer end groups) is determined by the solubility of the gold salt loaded dendrimer. Although we have extensively studied the structure of the hybrid formed under these maximal loading conditions, we have also investigated the variation of the structures formed with loading ratios below the maximum value. We have studied systems with gold ion to dendrimer end group ratios of 1:1, 1:2, and 1:4. UV−vis spectra for samples formed upon reduction are shown in Figure 2; SAXS results for the G9 sample are given in Figure 8. It can be seen from the SAXS data as well as from TEM (not shown) that a lower loading yields smaller particles. Gold diameters of 4, 3.3, and 2.5 nm (within ranges of ±0.2 nm) for 1:1, 1:2, and 1:4 loading are observed. Again, this corresponds well with the expected values for 2048, 1024, and 512 atoms.

In other polymer template systems, it has been observed that one part of the polymer particles ends up "fully" filled with gold while another part is completely empty, indicating a more complicated growth mechanism.[18] In contrast, with the dendrimers investigated here, the size of the metal colloids formed is precisely determined by the number of gold atoms that were added per dendrimer, introduced before as "fixed loading law".

Although one might be interested in putting as much gold as possible into a single dendrimer, the samples resulting from a lower loading also represent well-defined composite particles which may be of importance for certain applications. For example, dendrimer-stabilized metal colloids represent an interesting system for heterogeneous catalysis in aqueous solution. The hybrid particles containing smaller metal colloids may be more effective because of the larger surface area provided per mass or changed selectivity due to their different morphology.[9,31]

E. Effect of Dendrimer Generation on Colloid Size. Table 1 summarizes some TEM and SAXS results for hybrid structures obtained for different generation dendrimers under the same reduction conditions (1:1 loading, slow reduction). The effect of the dendrimer generation on the colloid size is not simple, i.e., for G2, the colloids formed are larger than those obtained with G4. For G6−G9 the gold diameter increases with increasing generation number. For G10, multiple smaller gold particles per dendrimer are formed. In the following paragraphs we describe the results of the particle characterization and discuss the different structures. In this context, one has to consider how the dendrimer structure itself changes with generation: G2 is a starlike molecule with 16 end groups; G3−G5 have starlike as well as spherelike features, and higher generation dendrimers show a spherical structure.[32]

For G2 and G4 dendrimers, gold colloids of 4 and 2 nm diameter, respectively, are detected by TEM as well as by SAXS. In addition, we observe the existence of larger dendrimer aggregates. For the G4 sample these have a well-defined dimension of 7 nm as evident from the pair distance distribution function as well as from our TEM staining experiments. Larger particles obtained with G2 rather than G4 dendrimer are in agreement with recent results from other authors who are studying these lower generation dendrimers as colloid stabilizers.[9] A schematic of multiple dendrimers attached to one gold colloid was inferred in that work but not verified experimentally. Small-angle scattering and Guinier analysis revealed aggregated structures formed upon colloid preparation using a G4 dendrimer by Beck Tan et al.[10] Thus, our results for low generation dendrimers are in agreement with the results of other authors.

The formation of multiple dendrimer aggregates may be understood because for these "small" molecules a single dendrimer cannot provide enough material to stabilize the surface of one gold colloid. In addition, very small metal clusters are less stable, so that colloids from the gold loading of more than one dendrimer are formed. This results in a hybrid structure of a metal colloid surrounded by several dendrimers. The colloid formation mechanism for these low generation dendrimers is different than for high generation dendrimers. The gold colloids are not formed inside a "preexisting container", but the nanostructure organizes only when the colloid is produced chemically. This resembles the concept of double-hydrophilic block copolymers in mineralization.[33,34] In contrast, the dendrimers are chemically

Table 1. Dendrimer Parameters and Experimental Results for the Generation-Dependent Experiments (Loading 1:1)

generation	M_w[a]	D(dendrimer),[b] nm	end groups[c]	D_{cal}(gold),[d] nm	D_{TEM}(gold),[e] nm	$D_{SAXS(gold)}$,[f] nm	D_{SAXS}(total),[g] nm
2	3 256		16	0.8	4.0	4.0	>20
4	14 215	4.5	64	1.3	~1.8	~2.0	7
5	28 788	6.5	128	1.6	~2.0	*h*	*i*
6	57 788	7.1	256	2.0	~2.0	~2.2	*i*
7	116 314	8.5	512	2.5	2.5	2.5	8.5
8	223 076	10.9	1024	3.2	3.2	3.2	11.0
9	466 546	13.2	2048	4.0	4.0	4.0	13.0
10	933 492	15.0	4096	5.1	*j*	3.0	14.0

[a] Theoretical molecular mass of the dendrimer in g/mol. [b] Diameter estimated from the radius of gyration as reported previously.[17] [c] Theoretical number of dendrimer end groups. [d] Calculated diameter of a gold particle consisting of this number of atoms. [e] Experimental diameter of the gold as estimated from TEM (within a range of ±0.2 nm). [f] Experimental diameter of the gold as estimated from SAXS. [g] Experimental total diameter of the hybrid structure as estimated from SAXS. (The uncertainty associated with the resolution of the scattering experiment is 0.7 nm.) [h] Not determined. [i] Aggregates. [j] Multiple 3 nm.

uniform, and no complex architectures result. From this point of view, the colloid stabilization can be considered as an analogue to the classical stabilization mechanism with low molar mass molecules such as citric acid.[35] The molecules can become attached to the colloid surface and act as stabilizers, but they do not template the colloid.

While the analysis of the G5 hybrid structure proved to be more difficult, for the G6 sample, a gold colloid of about 2 nm diameter is observed; thus, the size corresponds to 1:1 loading. However, the dendrimers at least partially aggregate in solution in this case. For G7−G9, individual dendrimer molecules containing single gold colloid particles are found. The TEM for the G8 sample is shown in Figure 9a. The structure of the hybrid particles corresponds to the G9 sample discussed before. SAXS scattering data are shown in Figure 10a. Pair distance distribution functions obtained from data for G7, G8, and G9 (Figure 10b) show the increasing gold colloid size with increasing dendrimer size. The colloid diameters of 2.5, 3.2, and 4 nm (within ranges of ±0.2 nm) agree well with the expected sizes.

The mid-generation dendrimers (G6−G9) obviously offer the best conditions in terms of a "host−guest nanoscale" synthesis. This may be explained by the fact that their structure provides sufficient polymer to stabilize the surface of the forming colloidal particle, along with enough flexibility for the growth of only one particle from all of the gold ions loaded in the dendrimer. Thereby, the number of gold atoms that build one colloid can be precisely controlled with these dendrimers ("fixed loading law").

For G10, multiple smaller gold particles inside one dendrimer are observed in the TEM (Figure 9b). In addition, the decreased gold diameter in comparison to the G9 sample is evident in the $P(r)$ function (Figure 10b, dotted line). In general, the growth of a colloid is determined by the free energy of the crystal formation and surface tension. However, when the colloid grows inside a polymeric matrix, the elastic forces of the surrounding polymer become important. The growth of a nucleated colloid is limited by the finite extension of neighboring polymer chains. In this context, one must note that with each generation number G the mass of the dendrimer is roughly doubled, while the size increases only linearly (mass: $M_w \sim 2^G$; radius: $R \sim G$; volume: $V \sim G^3$; compare Table 1). This means, as the generation number increases, the internal dendrimer segment density increases slightly,[32] and the flexibility of the dendrimer chains decreases. The volume of a single gold nanocluster would double with each generation, yet the space available for its formation would decrease. For the G10 dendrimer, it may be that the chain flexibility is not sufficiently high to allow for the growth of one colloidal particle. On the other hand, the increased surface to be stabilized for multiple smaller particles is likely to be provided by the G10 dendrimer. From this point of view, the G10 dendrimer still realizes a host−guest nanotemplating, and the different dendrimer structure results in a different colloid morphology. Similarly, in microgels of high cross-linking density only multiple small colloid particles can be formed, while the larger flexibility of lower cross-linking density

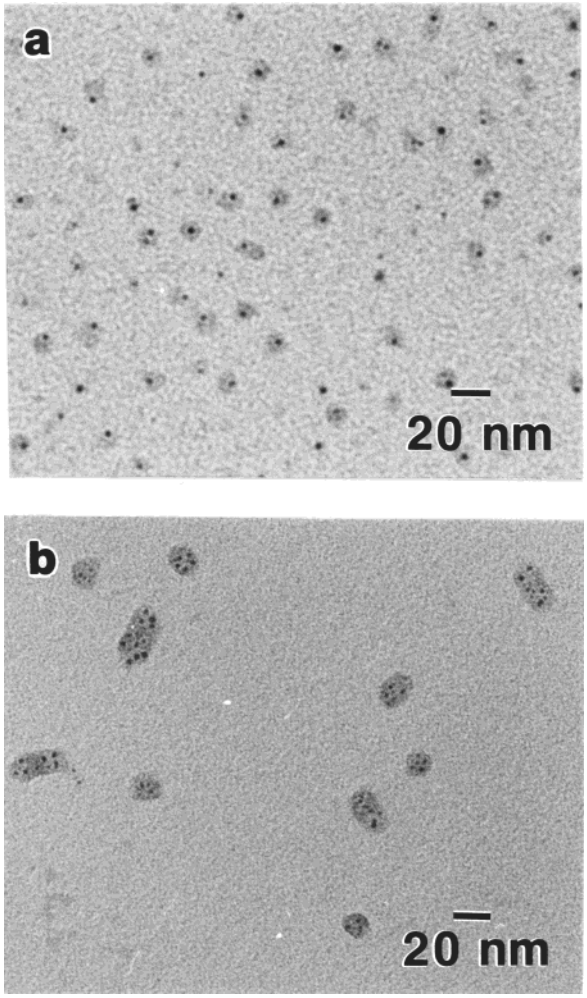

Figure 9. (a) TEM of gold containing G8 PAMAM dendrimer obtained for 1:1 loading and slow reduction. (The dendrimer has been stained with phosphotungstic acid.) (b) TEM of gold containing G10 PAMAM dendrimer obtained for 1:1 loading and slow reduction. (The dendrimer has been stained with phosphotungstic acid.)

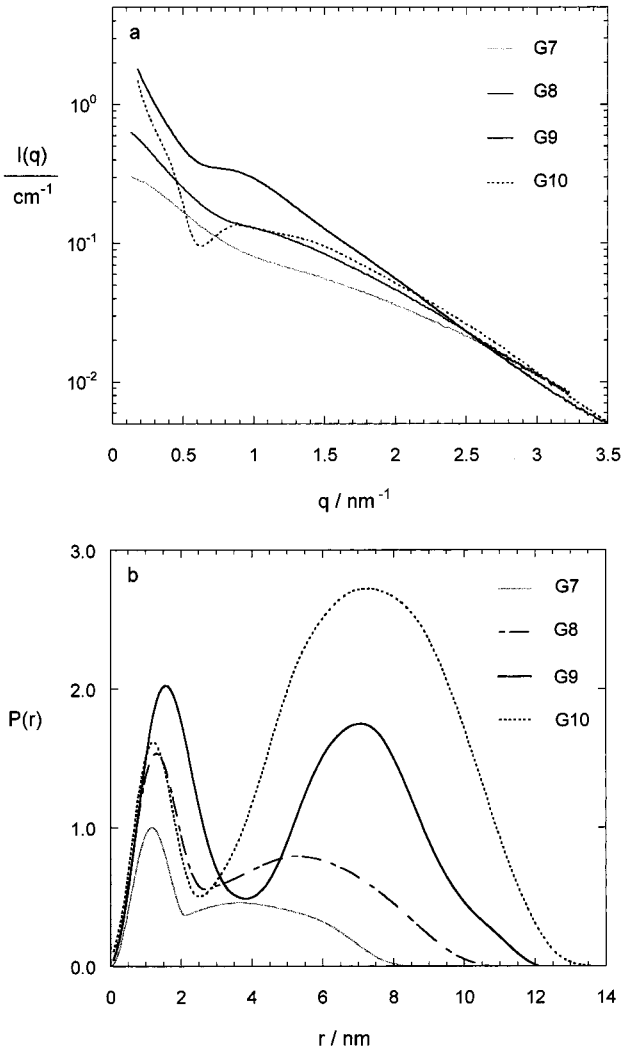

Figure 10. (a) Small-angle X-ray scattering curves $I(q)$ for gold−dendrimer hybrid structures obtained with PAMAM dendrimers of generation 7−10. The relative standard deviation in the SAXS intensity values in the range 0.2 $nm^{-1} < q <$ 1.6 nm^{-1} is less than 3%. At higher wavevectors, the relative standard deviation increases with q to a maximum value of 7%. (Data were collected up to a maximum value of the scattering vector magnitude $q = 4.4$ nm^{-1}. To allow for a better comparison of the features, data are plotted here only up to a maximum value of $q = 3.5$ nm^{-1}.) (b) Pair distance distribution functions $P(r)$ obtained by indirect Fourier transformation of the scattering data $I(q)$ in (a). For G7−G9 (solid lines) an increasing gold diameter with increasing dendrimer diameter is seen. Contrary, for G10 (dotted line) the gold diameter is decreased though the dendrimer diameter is further increased. The relative standard deviation in the $P(r)$ values is less than 3%.

microgels allows for the formation of continuous structures through the microgel.[18] But for the case of dendrimer nanotemplates, the "fixed-loading law" remains valid. About four 3 nm gold colloids inside one G10 dendrimer are formed, which is in good agreement with the expected amount of 4096 atoms.

While a detailed study has been presented on the parameters that influence the colloid formation for the reduction of gold salt, we have also synthesized other metal colloids such as copper, silver, and platinum inside the dendrimers as well as cadmium sulfide nanoclusters, which will be the subject of future reports. The examples demonstrate that the dendrimer nanotemplating is not restricted to a specific chemistry, but it represents a fundamental mechanism, which may be widely applied.

IV. Conclusions

PAMAM dendrimers are shown to be effective as nanotemplates of gold colloids. They not only stabilize the colloidal metal in aqueous solution but also determine the architecture of the forming nanostructures. G2−G4 dendrimers behave like low molecular mass colloid stabilizers; i.e., several dendrimers surround the surface of the metal particle formed. G6−G10 dendrimers act as effective "polymeric" nanotemplates. Metal particles are completely formed inside individual dendrimers, a template mechanism known as "host−guest nanoscale synthesis" or "exotemplating".[18,36] For G6−G9, one metal particle is formed in one dendrimer molecule. It is located offset from the center of the dendrimer. Without changing this hybrid-particle morphology, the size of the inorganic colloid can be precisely controlled by the number of precursor ions added per dendrimer ("fixed loading law"), i.e., via dendrimer generation or loading ratio. For G10, multiple colloids within one dendrimer molecule are formed due to the more crowded volume inside the dendrimer. To our knowledge, this is the first time such a transition has been shown from colloid "stabilization" by low molecular mass molecules to "polymer nanotemplating" with increase of molecular mass but unchanged chemistry of the stabilizing species.

The nanocluster-containing dendrimers represent well-defined hybrid particles that may be important for multiple applications, due to their unique catalytic selectivity[8,11,16] and potentially special optical and electrical behavior. They may further pave the way to new solid or surface materials, which combine the mechanical properties of polymers with special colloidal effects.

Acknowledgment. This material is based upon work supported in part by the U.S. Army Research office under Contract 35109-CH. We thank Donald Tomalia of MMI for providing us with dendrimers. SAXS measurements were carried out at the Advanced Polymer Beamline X27C at the National Synchrotron Light Source, Brookhaven National Laboratory. We thank Feng-Ji Yeh and Lizhi Liu for steady help with the SAXS setup. Franziska Gröhn thanks Ginam Kim for help in using the TEM and Heimo Schnablegger for important discussions about scattering data.

References and Notes

(1) Antonietti, M.; Göltner, C. *Angew. Chem., Int. Ed. Engl.* **1997**, *36*, 910.
(2) Jansen, J. F. G. A.; de Brabander-van den Berg, E. E. M.; Meijer, E. W. *Science* **1994**, *266*, 1226.
(3) Jansen, J. F. G. A.; Meijer, E. W. *J. Am. Chem. Soc.* **1995**, *117*, 4417.
(4) Zhao, M.; Sun, L.; Crooks, R. M. *J. Am. Chem. Soc.* **1998**, *120*, 4877.
(5) Esumi, K.; Suzuki, A.; Aihara, N.; Usui, K.; Torigoe, K. *Langmuir* **1998**, *14*, 3157.
(6) Balogh, L.; Tomalia, D. A. *J. Am. Chem. Soc.* **1998**, *120*, 7355.
(7) Sooklal, K.; Hanus, L. H.; Ploehn, H. J.; Murphy, C. J. *Adv. Mater.* **1998**, *10*, 1083.
(8) Zhao, M. Q.; Crooks, R. M. *Angew. Chem., Int. Ed. Engl.* **1999**, *38*, 364.
(9) Garcia, M. E.; Baker, L. A.; Crooks, R. M. *Anal. Chem.* **1999**, *71*, 256.
(10) Beck Tan, N. C.; Balogh, L.; Trevino, S. F.; Tomalia, D. A.; Lin, J. S. *Polymer* **1999**, *40*, 2537.
(11) Zhao, M.; Crooks, R. M. *Adv. Mater.* **1999**, *11*, 217.
(12) Zhao, M.; Crooks, R. M. *Chem. Mater.* **1999**, *11*, 3379.

(13) He, J. A.; Valluzzi, R.; Yang, K.; Dolukhanyan, T.; Sung, C.; Kumar, J.; Tripathy, S. K.; Samuelson, L.; Balogh, L.; Tomalia, D. A. *Chem. Mater.* **1999**, *11*, 3268.
(14) Esumi, K.; Suzuki, A.; Yamahira, A.; Torigoe, K. *Langmuir* **2000**, *16*, 2604.
(15) Esumi, K.; Hosoya, T.; Suzuki, A.; Torigoe, K. *Langmuir* **2000**, *16*, 2978.
(16) Crooks, R. M.; cited in: Meeting Report, *Science* **1999**, *283*, 165.
(17) Prosa, T. J.; Bauer, B. J.; Amis, E. J.; Tomalia, D. A.; Scherrenberg, R. *J. Polym. Sci.* **1997**, *35*, 2913.
(18) Antonietti, M.; Gröhn, F.; Hartmann, J.; Bronstein, L. *Angew. Chem., Int. Ed. Engl.* **1997**, *36*, 2080.
(19) Certain commercial materials and equipment are identified in this article in order to specify adequately the experimental procedure. In no case does such identification imply recommendation by the National Institute of Standards and Technology, nor does it imply that the material or equipment identified is necessarily the best available for this purpose.
(20) The accepted SI unit of concentration, mol/L, has been represented by the symbol M in order to conform the conventions of this journal.
(21) Hammouda, B.; Krueger; S.; Glinka, C. *J. Res. Natl. Inst. Stand. Technol.* **1993**, *98*, 31.
(22) Hsiau, B. S.; Chu, B.; Yeh, F. *NSLS Newsletter* July 1, 1997.
(23) Glatter, O. *Acta Phys. Austriaca* **1977**, *47*, 83.
(24) Glatter, O. *J. Appl. Crystallogr.* **1977**, *10*, 415.
(25) Glatter, O. *J. Appl. Crystallogr.* **1980**, *13*, 7, 577.
(26) Ottaviani, M. F.; Bossman, S.; Turro, N. J.; Tomalia, D. A. *J. Am. Chem. Soc.* **1994**, *116*, 661.
(27) Ottaviani, M. F.; Montalti, F.; Turro, N. J.; Tomalia, D. A. *J. Phys. Chem. B* **1997**, *101*, 158.
(28) Vassilev, K.; Ford, W. T. *J. Polym. Sci., Part A* **1999**, *37*, 2727.
(29) Antonietti, M.; Wenz, E.; Bronstein, L.; Seregina, M. *Adv. Mater.* **1995**, *7*, 12.
(30) Jackson, C. L.; Chanzy, H. D.; Booy, F. P.; Drake, B. J.; Tomalia, D. A.; Bauer, B. J.; Amis, E. J. *Macromolecules* **1998**, *31*, 6259.
(31) Klingelhöfer, S.; Heitz, W.; Greiner, A.; Oestreich, S.; Förster, S.; Antonietti, M. *J. Am. Chem. Soc.* **1997**, *119*, 10116.
(32) Prosa, T. J.; Bauer, B. J.; Amis, E. J., submitted for publication.
(33) Cölfen, H.; Antonietti, M. *Langmuir* **1998**, *14*, 582.
(34) Antonietti, M.; Breulmann, M.; Göltner, C.; Cölfen, H.; Wong, K. W. W.; Walsh, D.; Mann, S. *Chem. Eur. J.* **1998**, *4*, 2493.
(35) Such colloidal stabilization was already applied by Faraday in the 1850s. A recent overview is given by: Kreibig, U.; Vollmer, M. *Optical Properties of Metal Clusters*; Springer: Heidelberg, 1995.
(36) Mann, S. *Biomimetic Materials Chemistry*; VCH: Weinheim, 1996.

MA000149V